AMERICAN SOCIETY FOR MICROBIOLOGY | mBio®

RESEARCH ARTICLE
Host-Microbe Biology

Targeting mTOR with MLN0128 Overcomes Rapamycin and Chemoresistant Primary Effusion Lymphoma

Carolina Caro-Vegas,[a,b] Aubrey Bailey,[a] Rachele Bigi,[a] Blossom Damania,[a,b] Dirk P. Dittmer[a,b]

[a]UNC Lineberger Comprehensive Cancer Center, University of North Carolina, Chapel Hill, North Carolina, USA
[b]Department of Microbiology and Immunology, University of North Carolina, Chapel Hill, North Carolina, USA

ABSTRACT Primary effusion lymphoma (PEL) is caused by Kaposi's sarcoma-associated herpesvirus (KSHV). PEL has a highly active mTOR pathway, which makes mTOR a potential therapeutic target. MLN0128 is an ATP-competitive inhibitor of mTOR that has entered clinical trials for solid tumors. Our results demonstrated that MLN0128 has a greater effect on inhibiting proliferation than the allosteric mTOR inhibitor rapamycin. MLN0128 has ~30 nM 50% inhibitory concentration (IC_{50}) across several PEL cell lines, including PEL that is resistant to conventional chemotherapy. MLN0128 induced apoptosis in PEL, whereas rapamycin induced G_1 arrest, consistent with a different mechanism of action. MLN0128 inhibited phosphorylation of mTOR complex 1 and 2 targets, while rapamycin only partially inhibited mTOR complex 1 targets. PEL xenograft mouse models treated with MLN0128 showed reduced effusion volumes in comparison to the vehicle-treated group. Rapamycin-resistant (RR) clones with an IC_{50} for rapamycin 10 times higher than the parental IC_{50} emerged consistently after rapamycin exposure as a result of transcriptional adaptation. MLN0128 was nevertheless capable of inducing apoptosis in these RR clones. Our results suggest that MLN0128 might offer a new approach to the treatment of chemotherapy-resistant PEL.

IMPORTANCE Primary effusion lymphoma (PEL) is an aggressive and incurable malignancy, which is usually characterized by lymphomatous effusions in body cavities without tumor masses. PEL has no established treatment and a poor prognosis, with a median survival time shorter than 6 months. PEL usually develops in the context of immunosuppression, such as HIV infection or post-organ transplantation. The optimal treatment for PEL has not been established, as PEL is generally resistant to traditional chemotherapy. The molecular drivers for PEL are still unknown; however, PEL displays a constitutively active mammalian target of rapamycin (mTOR) pathway, which is critical for metabolic and cell survival mechanisms. Therefore, the evaluation of novel agents targeting the mTOR pathway could be clinically relevant for the treatment of PEL.

KEYWORDS INK128, Kaposi's sarcoma-associated herpesvirus, MLN0128, sapanisertib, everolimus, lymphoma, mTOR, rapamycin, sirolimus

Primary effusion lymphoma (PEL) is a non-Hodgkin B-cell lymphoma that is associated with infection by Kaposi sarcoma-associated herpesvirus (KSHV) (1). PEL typically presents as lymphomatous effusions in body cavities, most commonly in the pleural, pericardial, and peritoneal cavities. This lymphoma generally develops in the context of immunosuppression, such as during HIV infection or organ transplantation (2). Currently, PEL is treated with a chemotherapeutic regimen containing cyclophosphamide, doxorubicin, vincristine, and prednisolone (CHOP). Resistance develops rapidly, with a median survival time of 6.2 months (3, 4). Hence, there exists an urgent need to develop novel and targeted therapies for PEL.

Citation Caro-Vegas C, Bailey A, Bigi R, Damania B, Dittmer DP. 2019. Targeting mTOR with MLN0128 overcomes rapamycin and chemoresistant primary effusion lymphoma. mBio 10:e02871-18. https://doi.org/10.1128/mBio.02871-18.

Editor Thomas Shenk, Princeton University

Address correspondence to Dirk P. Dittmer, dirk_dittmer@med.unc.edu.

This article is a direct contribution from a Fellow of the American Academy of Microbiology. Solicited external reviewers: Dean Kedes, University of Virginia; Jae Jung, University of Southern California.

Received 20 December 2018
Accepted 2 January 2019
Published 19 February 2019

PEL are addicted to the mammalian target of rapamycin (mTOR) signaling pathway. All PEL tested display constitutively active mTOR (5, 6). The mTOR pathway controls cell growth, metabolism, proliferation, angiogenesis, and survival (reviewed in reference 7) and is activated in a large number of cancers. In nonviral cancers, this is often due to activating mutations upstream of mTOR and/or loss of tumor suppressors such as the phosphatase and tensin homolog (PTEN). In PEL, PTEN is intact but inactivated by phosphorylation (8). Several viral proteins, such as ORFK1 (K1) (9), ORFK2 (vIL6) (9), ORF45 (10), and ORF74 (vGPCR) (11–13), induce the mTOR pathway in PEL as well as in Kaposi's sarcoma (KS).

The mTOR kinase functions in two structurally and functionally distinct complexes designated mTOR complexes 1 (mTORC1) (14, 15) and 2 (mTORC2) (16, 17). mTORC1 targets p70-S6 kinase 1 (p70S6K1) and eukaryotic translation initiation factor 4E-binding protein 1 (4EBP1). mTORC1 phosphorylates p70S6K1 at Thr389, which in turn phosphorylates ribosomal protein S6 (RPS6), thereby promoting protein synthesis (18). mTORC1 also phosphorylates 4EBP1 at multiple sites, which causes dissociation from eukaryotic translation initiation factor 4E (eIF4E), promoting cap-dependent translation. mTORC2 phosphorylates Akt (also known as protein kinase B) at Ser473. Akt in turn activates mTORC1 through a positive-feedback loop (19, 20), as well as additional prosurvival proteins. Another mTORC2 target is SGK1. AKT and SGK1 are members of the AGC family of kinases. They have both distinct and overlapping roles (21, 22). mTORC2 phosphorylates SGK1 proteins at Ser422, as well as one of SGK1's physiological targets, N-myc downstream-regulated gene 1 (NDRG1) (23). Phosphorylation of these proteins represents the best understood biomarker of mTORC activity.

Rapamycin and its analogs (rapalogs) are allosteric inhibitors of mTORC1. We and others previously reported that rapamycin had preclinical activity against in PEL, as well as clinical efficacy against KS (5, 12, 24–26). Switching from cyclosporine to rapamycin has become the standard of care for transplant-associated KS. Unfortunately, rapamycin only arrests cells: it does not induce apoptosis, and resistance develops readily (27). While rapamycin always inhibits p70S6K1 and RPS6, its effect on 4EBP1 is more variable (28–30). Since rapamycin does not target mTORC2, this may result in a compensatory activation of Akt and mTORC2, at least until enough mTOR kinase is trapped in inactive rapamycin-FKBP-mTORC1 complexes to start depleting mTORC2 (31). These limitations triggered the development of second-generation, ATP-competitive inhibitors, which target both mTORC1 and mTORC2.

This is the study of an ATP-competitive inhibitor in PEL. We focused on MLN0128 (INK128 [sapanisertib]), rather than other ATP-competitive inhibitors, because MLN0128 is orally bioavailable and farthest along in clinical development (32–34). MLN0128 inhibited both mTORC1 and mTORC2 in PEL at a nanomolar 50% inhibitory concentration (IC_{50}) and induced rapid apoptosis rather than G_1 arrest. MLN0128 was efficacious against doxorubicin-resistant PEL, such as the BCP-1 isolate, as well as rapamycin-resistant PEL. Furthermore, MLN0128 had reproducible efficacy in PEL xenograft models. Based on these studies, the clinical evaluation of MLN0128 in PEL and KS seems warranted.

RESULTS

MLN0128 inhibits PEL proliferation. To compare MLN0128 and rapamycin, we tested several well-characterized PEL cell lines, such as BC-1 (KSHV and Epstein-Barr virus [EBV] positive) and BCBL-1 (KSHV positive, but EBV negative), across multiple experimental designs. (i) At 100 nM, MLN0128 inhibited PEL proliferation over time, as measured by trypan blue exclusion assay (Fig. 1A and B). (ii) MLN0128 abolished colony formation in soft agar. In contrast, rapamycin only reduced colony number to ~40% of the control for BCBL-1 (Fig. 1C and D) and ~20% of the control for BC-1 at the same concentration (see Fig. S1A and S1B in the supplemental material). (iii) CellTiter-Glo assay (CTG) confirmed the previously reported IC_{50} values for rapamycin (Fig. 1E; see Fig. S1C in the supplemental material). Of note, even at the highest concentration of rapamycin, there remained a resistant fraction of live cells, consistent with cell cycle

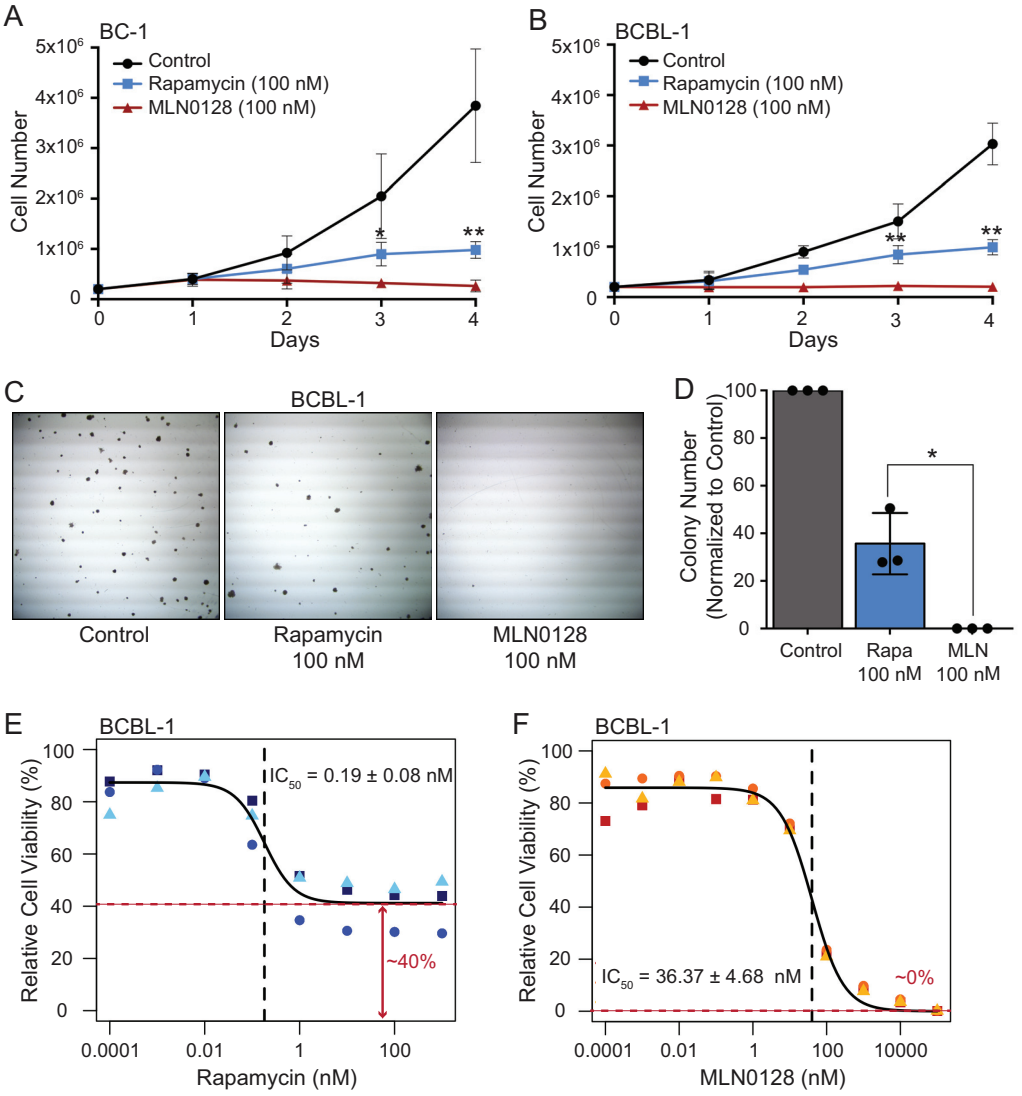

FIG 1 MLN0128 inhibits PEL proliferation. (A) BC-1 and (B to D) BCLB-1 cells were incubated with 100 nM rapamycin or MLN0128, and inhibition of cell proliferation was assessed by (A and B) trypan blue exclusion assay at the indicated times or (C and D) colony formation assay after 2 weeks. Data represent the mean ± standard deviation (SD) from $n = 3$ independent experiments (unpaired 2-tailed t test; *, $P < 0.05$, and **, $P < 0.01$, rapamycin versus MLN0128 group). BCBL-1 cells were treated with increasing concentrations of (E) rapamycin or (F) MLN0128 for 48 h, and cell viability was measured by CellTiter-Glo luminescent cell viability assay. Dose-response curves were generated as a percentage of the vehicle (100%) and no-cell control (0%) in R. Each data point represents the mean from independent wells ($n = 4$).

arrest (see Fig. S2 in the supplemental material). MLN0128 had low nanomolar concentration IC_{50} values in this assay ranging from 9.71 to 47.56 nM (Table 1). In contrast to rapamycin, no resistant fraction remained in MLN0128-treated cells (Fig. 1F; see Fig. S1D in the supplemental material). Compared to two other rapalogs, temsirolimus and ridaforolimus, with improved solubility, MLN0128 still showed a more complete

TABLE 1 MLN0128 IC_{50} values for a panel of 5 PEL cell lines

PEL cell line ($n = 3$)	IC_{50} (nM)
BC-1	16.20 ± 4.94
BCBL-1	37.43 ± 13.13
BC-3	47.56 ± 7.48
BCP-1	9.71 ± 0.76
BCBL-1TrexRTA-Luc	26.07 ± 5.15

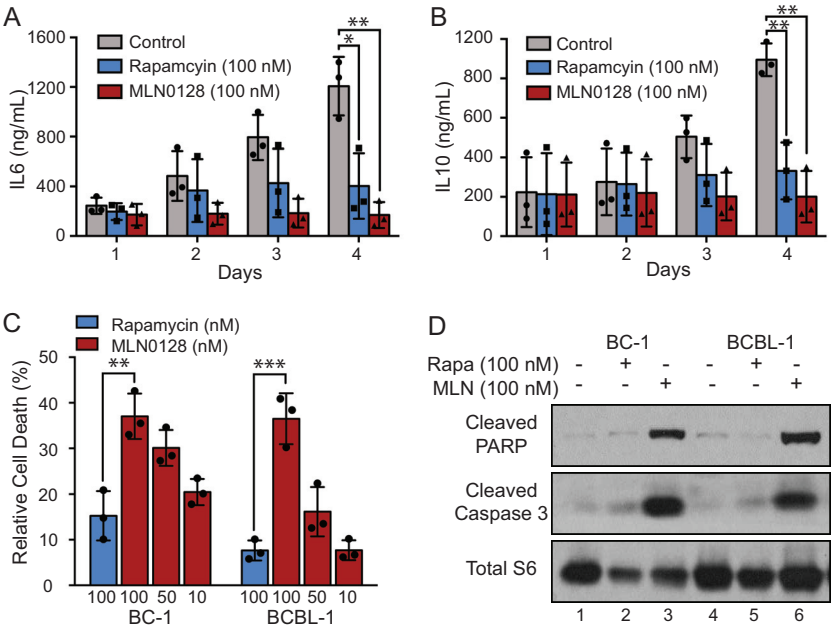

FIG 2 MLN0128 induces PEL apoptosis. (A and B) BC-1 cells were treated with 100 nM rapamycin or MLN0128 for the indicated times, (A) IL-6 and (B) IL-10 (PEL markers) on the supernatant were measured by ELISA. Data represent the mean ± SD from $n = 3$ independent experiments (unpaired 2-tailed *t* test; *, $P < 0.05$, **, $P < 0.01$, and ***, $P < 0.001$, control versus rapamycin or MLN0128 group). BC-1 and BCBL-1 cells were treated with the indicated concentration of rapamycin and MLN0128 for 48 h; cell apoptosis was measured by (C) annexin V fluorescence-activated cell sorter (FACS), where percentages indicate annexin V-positive cells (apoptotic) normalized to control, and (D) expression of cleaved PARP, cleaved caspase-3, and total S6 as the loading control. Data represent the mean ± SD from $n = 3$ independent experiments (unpaired 2-tailed *t* test; *, $P < 0.05$, **, $P < 0.01$, and ***, $P < 0.001$, rapamycin versus MLN0128 group). Western blots were repeated three times with similar results.

inhibition of PEL growth (Fig. S1E and S1F). All experiments were conducted at 0.00002% of dimethyl sulfoxide (DMSO), which up to 0.1% final concentration had no effect on cell growth (data not shown). (iv) Levels of interleukin-6 (IL-6) and IL-10 were evaluated as these cytokines correlate with PEL proliferation and may function as autocrine growth factors (35, 36). As reported previously, IL-6 and IL-10 were significantly reduced upon treatment with rapamycin. Treatment with MLN0128 showed even greater reduction (Fig. 2A and B). Importantly, when the data are normalized to the number of cells in each sample, the difference between IL-6 and IL-10 levels is not significant, which confirms IL-6 and IL-10 as markers for PEL proliferation. Whether in addition IL-10 is more directly sensitive to mTORC status remains the subject of further studies. These results demonstrate that MLN0128 inhibits PEL proliferation in a manner on par with or better than rapamycin, temsirolimus, and ridaforolimus.

MLN0128, but not rapamycin, induces apoptosis of PEL cell lines. To test the hypothesis that MLN0128 induced cell death, (i) we used annexin V/propidium iodide (PI) flow cytometry to quantify apoptosis at 48 h. MLN0128 induced significantly higher levels of annexin V-positive cells than rapamycin in a dose-dependent manner (Fig. 2C). Representative flow cytometric plots are shown in Fig. S3 in the supplemental material. (ii) Apoptosis was confirmed by Western blotting for cleaved poly(ADP-ribose) polymerase (PARP) and cleaved caspase-3, which are established markers of apoptosis (Fig. 2D). MLN0128 induced accumulation of cleaved PARP and cleaved caspase-3, while rapamycin did not. In sum, MLN0128 induced apoptosis, whereas rapamycin did not.

MLN0128 inhibits mTORC1 and mTORC2 signaling. To examine if MLN0128 inhibited mTORC1 and mTORC2 in PEL cells, phosphorylated and total levels of validated downstream targets of mTORC1 (rpS6 and 4EBP1) or mTORC2 (AKT and NGRD1) were measured. MLN0128 inhibited the phosphorylation of both mTORC1

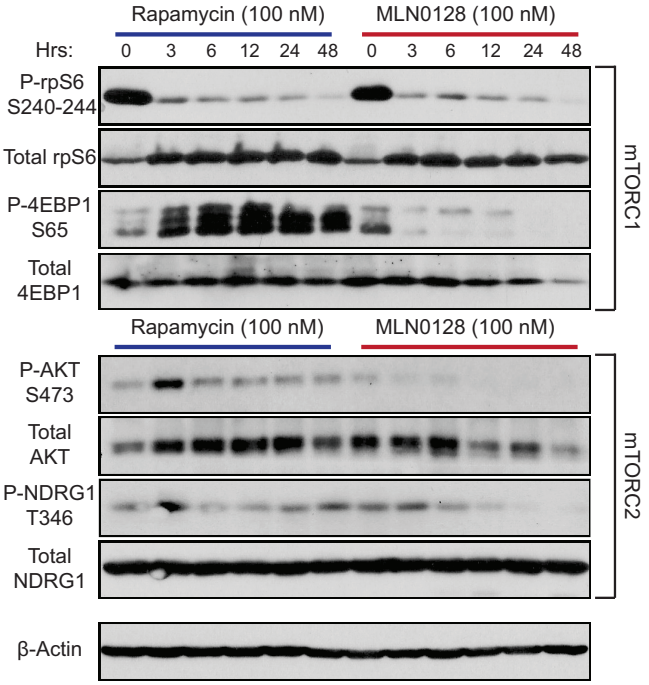

FIG 3 MLN0128 blocks both mTORC1 and mTORC2 in PEL. BCBL-1 cells were treated with 100 nM rapamycin or MLN0128 for 0 to 48 h, and regular and phospho levels of S6, 4EBP1, AKT, and NDGR1 were measured by Western blotting. β-Actin was used as a loading control for whole-cell extracts. Western blots were repeated three times with similar results.

targets, 4EBP1 (Ser65) and rpS6 (Ser240–244), as well as both mTORC2 targets, AKT (Ser473) and NDRG1 (Thr346) (Fig. 3). Rapamycin only partially inhibited mTORC1: phosphorylation of rpS6 was inhibited, yet 4EBP1 remained phosphorylated. As expected, rapamycin did not inhibit mTORC2. MLN0128 prevented feedback activation of AKT, while rapamycin led to the transient phosphorylation of AKT at Ser473 at 3 h. To confirm the specificity, we subjected MLN0128 to a high-throughput assay against 442 purified kinases (see Table S1 in the supplemental material) (37). MLN0128 was specific for mTOR at 25 nM, which was similar to the IC_{50} for PEL (see Fig. S4A in the supplemental material) (38). At 10,000 nM, MLN0128 showed a somewhat broader inhibition profile, similar to other mTOR/phosphatidylinositol 3-kinase (PI3K) ATP-competitive inhibitors, such as WYE354, pp242, NVP-BEZ235, and Torin1 (Fig. S4); however, this concentration is ~1,000× higher than that used here for PEL. With PEL being among the most mTOR-addicted lymphomas, the low IC_{50} for MLN0128 is consistent with primary inhibition of only mTOR kinase. These results establish that MLN0128 inhibits mTORC1 and mTORC2 activity without feedback activation of AKT.

MLN0128 inhibits PEL growth *in vivo*. To determine *in vivo* efficacy, we used an established xenograft model for PEL (5) augmented by live imaging. Unlike most other lymphomas, PEL grow as effusions in patients. Hence, an intraperitoneal (i.p.) model mimics the clinical presentation. MLN0128 reduced PEL progression of BCBL-1 and BCBL-1TrexRTA-Luc cells, as measured by effusion volume (Fig. 4A) and IL-6 levels (Fig. 4B). There was no significant difference between MLN0128 and rapamycin treatment (Fig. 4A). To study this further, in mice that no longer had overt effusions at the end of the observation period, the cavity was washed with phosphate-buffered saline (PBS) to collect any cells that may still be present on the cavity. Live cells were quantified and showed a significant difference between mice treated with rapamycin and those treated with MLN0128 (Fig. 4C). Weekly bioluminescence measurements showed a significant decrease in region of interest (ROI) luminescence with treatment (Fig. 4D and E; see Fig. S5A and S5B in the supplemental material). To confirm these results, positron emission tomography-computed tomography (PET-CT) was performed.

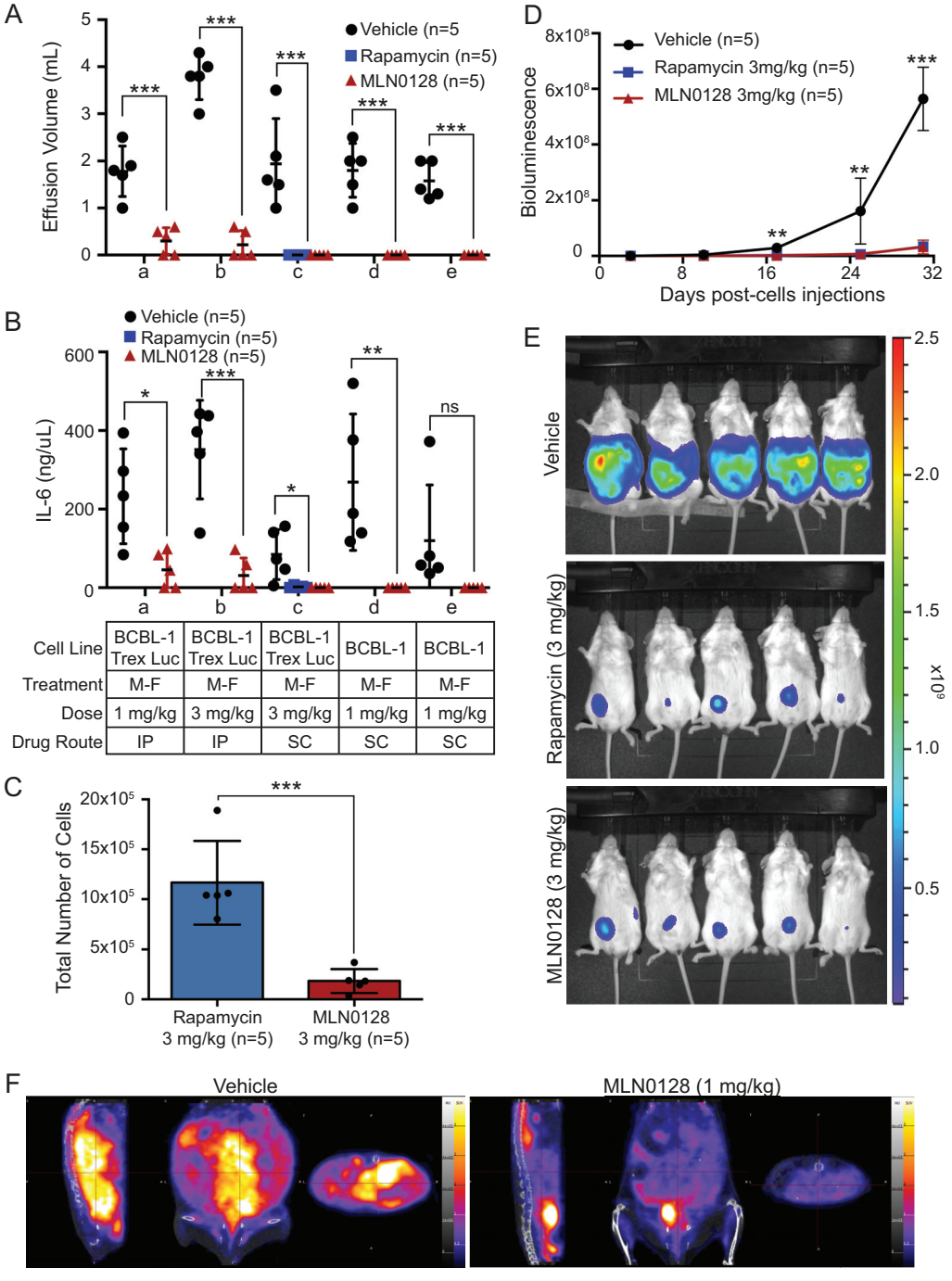

FIG 4 MLN0128 inhibits PEL growth in xenograft models. PEL xenograft models were treated with vehicle ($n = 25$ total), rapamycin ($n = 5$ total), or MLN0128 ($n = 25$ total) at the indicated concentration by i.p. or s.c. injections following a Monday to Friday dosing schedule for 4 weeks for BCBL-1TrexRTA-Luc or 8 weeks for BCBL-1 studies. In each of the experiments a to e, $n = 5$ for each treatment group. MLN0128-treated mice remained active and displayed no toxicity signs such as weight loss. (A) Effusions were harvested and quantified at the end of the study, and (B) IL-6 levels were measured by ELISA (unpaired 2-tailed *t* test; ns, not significant, *, $P < 0.05$, **, $P < 0.01$, and ***, $P < 0.001$, vehicle [$n = 5$] versus MLN0128 [$n = 5$] group or vehicle [$n = 5$] versus rapamycin [$n = 5$] per experiments a to e). (C) PEL cell quantification of PBS cavity wash from mice with no effusion from experiment c (unpaired 2-tailed *t* test; *, $P < 0.05$, **, $P < 0.01$, and ***, $P < 0.001$, MLN0128 [$n = 5$] versus rapamycin [$n = 5$] group). (D) Representative bioluminescent quantification of BCBL-1TrexRTA-Luc studies. (E) Representative image of bioluminescence imaging of BCBL-1TrexRTA-Luc studies and (F) PET-CT of BCBL-1 studies.

This showed a significant decrease in tumor metabolism between the treated and vehicle groups normalized to pretreatment conditions (Fig. 4F; see Fig. S5C to S5E and Movies S1 and S2 in the supplemental material). To verify that the effusion contained PEL cells rather than mouse cells, we performed Giemsa staining, which showed cells

within the effusion had PEL-like features, such as a prominent pleomorphic nucleoli and increased size compared to mouse cells (see Fig. S5F to S5H in the supplemental material). MLN0128 did not cause mortality or evident toxicity, demonstrated by constant body weight (see Fig. S6 in the supplemental material); the treated mice remained active throughout the experiment. This demonstrates that MLN0128 inhibits PEL *in vivo*.

MLN0128 induces apoptosis in rapamycin-resistant PEL. To test the hypothesis that MLN0128 was active against rapamycin-resistant (RR) PEL, we generated RR PEL, by culturing BCBL-1TrexRTA-Luc in increasing concentrations of rapamycin for 3 months, followed by colony formation assay and single-colony isolation. MLN0128 did not yield any colonies under the same schedule. Each of three RR clones exhibited a 6-fold increase in rapamycin IC_{50} compared to parental cells (Fig. 5A and B). The surviving fraction increased ~20% to ~60% in the RR compared to the parental clone. Even though the MLN0128 IC_{50} had a 2-fold increase between the parental and RR clones, MLN0128 was still effective at decreasing PEL viability to 0% in all RR clones (Fig. 5C and D). Additionally, MLN0128 induced apoptosis in both RR and parental clones to a similar degree (Fig. 5E). Exome sequencing of both parental and RR clones did not uncover mutations in the genes coding for mTOR or FKBP1 or other known genes in the mTOR pathway. To test whether transcriptional changes correlated with rapamycin resistance, we performed transcriptome sequencing (RNA-seq). Principal-component analysis uncovered significant and consistent differences between three parental and three RR clones (see Fig. S7A in the supplemental material). The most consistent change was the upregulation of IL-10 in the RR clones (Fig. 5G; see Fig. S7B in the supplemental material). This was also reflected at the protein level since the RR clones exhibited an ~100-fold increase of secreted IL-10 by comparison to the parental clones (Fig. 5F). In sum, MLN0128 is efficacious even against RR PEL.

DISCUSSION

PEL is a particularly aggressive type of post-germinal center B cell lymphoma, which is caused by KSHV and which manifests as liquid effusions in body cavities. Prognosis is poor, and resistance to conventional chemotherapy develops quickly. A defining feature of PEL is their dependence on PI3K/Akt/mTOR signaling, which seems to be driven by viral proteins rather than activating mutations in this pathway. Consequently, mTOR inhibitors such as rapamycin (5) and PI3K/mTOR inhibitors such as NVP-BEZ235 (6) show preclinical efficacy. Unfortunately, NVP-BEZ235 was too toxic clinically (39, 40), and rapamycin was cytostatic rather than cytotoxic for PEL. While this suffices for rapamycin to control KS (24, 26) and to yield a clinical benefit in mantle cell lymphoma and renal cancer, it limits its use against a highly aggressive lymphoma such as PEL. Of note, the orally bioavailable rapamycin derivative everolimus was clinically efficacious against advanced renal cell carcinoma patients, who progressed on pan-receptor tyrosine kinase inhibitors, such as sunitinib or sorafenib (41). This is consistent with mTOR being downstream of vascular endothelial growth factor (VEGF) receptors, which are targeted by broad-spectrum receptor tyrosine kinase inhibitors, and which are known oncogenic drivers in PEL and KS.

MLN0128 is an orally bioavailable, ATP-competitive inhibitor that targets mTORC1 and mTORC2. It showed promise in preclinical studies and has passed phase 1 trials in multiple myeloma, non-Hodgkin's lymphoma, and Waldenström's macroglobulinemia (32). This study established preclinical efficacy and mechanism of action for MLN0128 in PEL. MLN0128 had an IC_{50} of 10 to 50 nM across multiple PEL cell lines (Table 1). This effective concentration is in range of currently approved cytotoxic agents for PEL (e.g., doxorubicin), as well as rapamycin/everolimus. While there are many targeted agents under consideration against KSHV-associated cancers, the only ones that demonstrated some clinical efficacy in KS had similar low nanomolar concentration IC_{50}s in the PEL culture system. In the absence of a KS tumor model, inhibition of PEL growth in culture and in xenografted mice represents the most stringent preclinical model for testing novel agents.

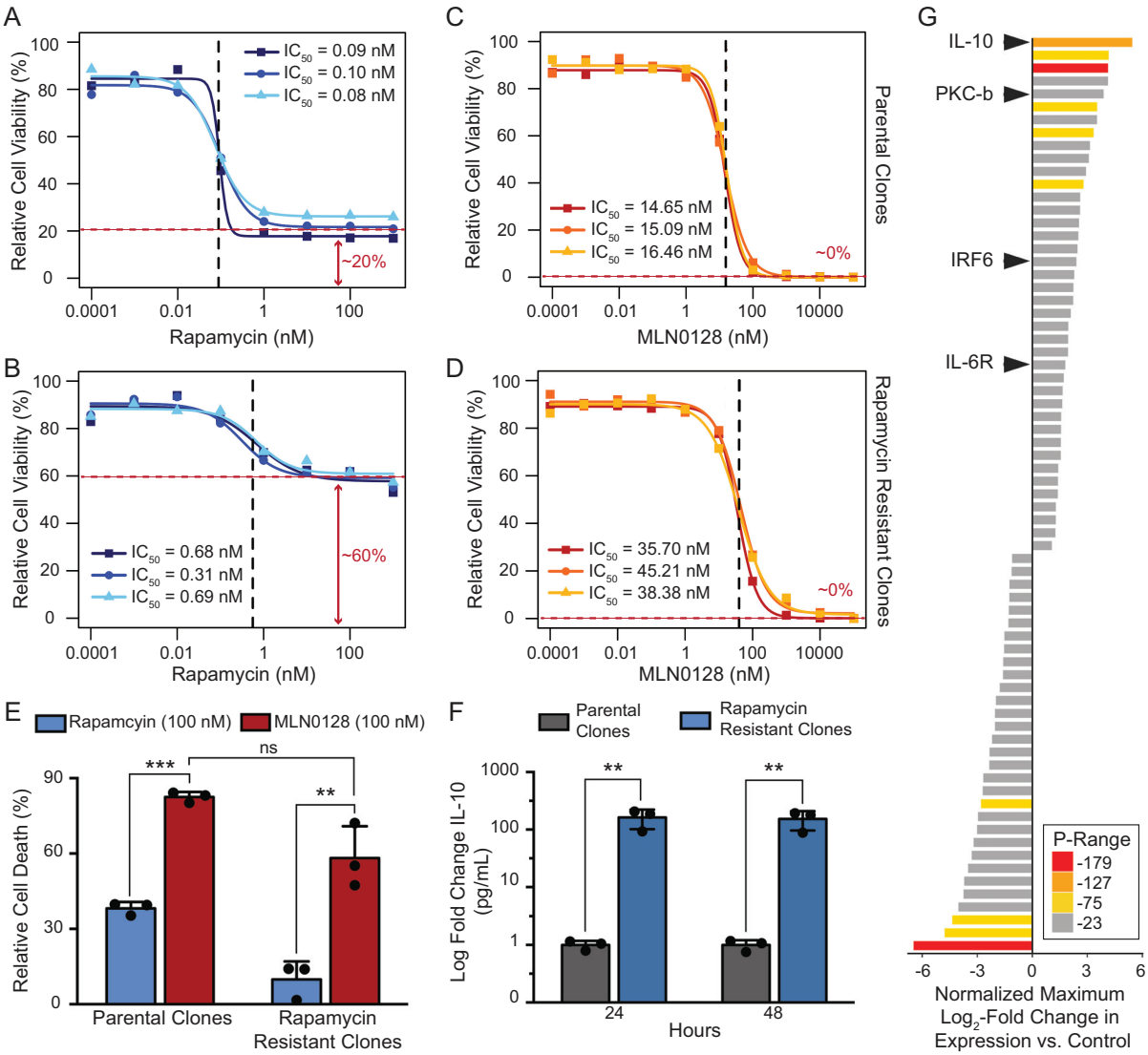

FIG 5 MLN0128 induces apoptosis of rapamycin-resistant clones. (A and C) Parental and (B and D) rapamycin-resistant clones were treated with increasing concentrations of (A and B) rapamycin or (C and D) MLN0128 for 48 h, and cell viability was measured by CellTiter-Glo luminescent cell viability assay. Dose-response curves were generated as a percentage of the vehicle (100%) and the no-cell control (0%) in R. The IC_{50}s (95% confidence interval) are shown by panel as follows: (A and B) rapamycin treatment of (A) the parental clones, 1, 0.09 ± 0.04, 2, 0.10 ± 0.03, and 3, 0.08 ± 0.02 nM; (B) rapamycin-resistant clones, 1, 0.68 ± 0.75, 2, 0.31 ± 0.24, and 3, 0.69 ± 0.88 nM; (C and D) MLN0128 treatment of (C) the parental clones, 1, 14.65 ± 3.10, 2, 15.09 ± 2.80, and 3, 16.46 ± 5.25 nM; and (D) rapamycin-resistant clones, 1, 35.70 ± 5.50, 2, 45.21 ± 8.90, and 3, 38.39 ± 7.82 nM. Data represent the mean from $n = 4$ independent wells. (E) Parental and rapamycin-resistant clones were treated with 100 nM rapamycin or MLN0128 for 48 h. Cell apoptosis was measured by annexin V FACS; the percentages indicate annexin V-positive cells (apoptotic) normalized to the control. (F) Levels of IL-10 were measured by ELISA in parental and RR clones after 24 or 48 h of seeding time. Data represent the mean ± SD from $n = 3$ independent clones (unpaired 2-tailed t test; ns, not significant, **, $P < 0.01$, and ***, $P < 0.001$, rapamycin versus MLN0128 group). (G) The RNA profile of parental and rapamycin-resistant clones was obtained by RNA-seq analysis.

Importantly, the action of MLN0128 was effective against a doxorubicin-resistant PEL cell line, BCP-1: i.e., MLN0128 was independent of p53 mutation status in PEL (42). MLN0128 induced apoptosis, whereas rapamycin and its analogs only induced cell cycle arrest (Fig. 2). MLN0128 effectively inhibited mTORC1 and mTORC2 activity, while rapamycin caused a transient increase in Akt S473 phosphorylation, due to a feedback loop, indicating the presence of active mTORC2 (31) (Fig. 3). There are various models that may explain the greater efficacy of MLN0128. Most likely, the dual inactivation of both mTORC1 and mTORC2 by MLN0128 might explain its greater effect on PEL compared to rapamycin. This would also disrupt the compensatory upregulation of mTORC2 in response to mTORC1 inhibition as observed in solid tumors. Another

explanation could be that the allosteric inhibitor rapamycin only inhibited some of the downstream pathways of mTORC1, whereas the ATP-competitive mTORC inhibitors tend to have a far broader effect on mTORC1 substrates (30). A third possibility could involve differential intracellular accumulation and pharmacology between rapamycin derivatives and MLN0128. Lastly, rapamycin has been shown to inhibit KSHV reactivation, specifically replication and transcription activator (RTA) function (43). We have not tested it, but presumably MLN0128 would do so as well and more completely. This in turn may downregulate RTA-dependent oncoproteins of KSHV such as vGPCR (12, 13) or the viral protein kinase orf36, which is a functional homolog of p70S6K (44). As PEL (and KS) are extraordinarily sensitive to mTORC inhibitors, the detailed study of these compounds in PEL may yield further mechanistic insights into their mechanism of action.

MLN0128 was active *in vivo* at 1 mg/kg of body weight/day (Fig. 4) and showed no toxicity. As previously noted, PEL develops resistance to rapamycin overtime. In culture, we were able to shift the IC_{50} for rapamycin by 100-fold within 3 months, while under the same condition, resistance to MLN0128 only changed 2-fold. The differential effect in PEL may be explained by the cytostatic activity of rapamycin, which gives PEL the chance to develop resistance. On the other hand, MLN0128 induces rapid apoptosis and therefore makes the development of resistance more difficult. Of note, we did not recover any previously described mutations in the RR clones, such as mutations in FKBP. Our screen was limited as we only sequenced a few resistant isolates. At the same time, all the RR clones tested had an upregulation of IL-10 at the transcriptional and protein levels. This was consistent with the rapid adaptation in culture, rather than selection for resistance mutants. It may elucidate a mechanism of rapamycin resistance analogous to the role IL-7 plays in mediating resistance to rapamycin in preclinical models of B cell leukemia (45). Importantly, MLN0128 was active against RR PEL (Fig. 5). In toto, these studies establish the mechanism of action for MLN0128 in this lymphoma and suggest that clinical studies of MLN0128 in PEL and KS are warranted.

MATERIALS and METHODS

Compounds and cell culture. MLN0128 and rapamycin were purchased from Selleckchem. Compounds were dissolved in DMSO (Sigma-Aldrich), aliquoted, and stored at −80°C. Cell lines were cultured in RPMI 1640 supplemented with 100 U/ml penicillin-streptomycin (Thermo Fisher), 2 mM L-glutamine (Thermo Fisher), and 10% fetal bovine serum (FBS) (Sigma-Aldrich), maintained at 37°C in 5% CO_2, and passaged for no more than 3 months. BC-1, BCBL-1, BC-3, and BCP-1 were obtained from ATCC. BCBL-1TrexRTA cells were a gift from J. Jung (46). RedFect (Perkin Elmer) was used to confer continuous red-luciferase expression (BCBL-1TrexRTA-luc), and cells were maintained in hygromycin B (20 μg/ml) and puromycin (1.25 μg/ml). Cell lines were authenticated by NextGen-based HLA and short tandem repeat (STR) typing (https://www.med.unc.edu/vironomics) and found free of mycoplasma by the Mycoalert mycoplasma test kit (Lonza).

Cell proliferation and cell viability. Cells were cultured at indicated concentration of inhibitor and counted in octuplicates using trypan blue (Sigma). Cell viability was determined at 48 h by CellTiter-Glo Assay (Promega) as per the manufacturer's instructions. Luminescence was measured at 560 nm using FLUOstar Optima (BMG Lab Tech). IC_{50}s were calculated using R.

Colony formation. Cells were plated in triplicates in 10% FBS complete RPMI medium with 1% methylcellulose containing the indicated concentration of inhibitor. Colonies were counted after 2 weeks using a Leica MZ 6 microscope.

Apoptosis and cell cycle. Cell were treated the indicated concentration of inhibitor and incubated for 24, 48, 72, and 96 h. For the apoptosis assay, cells were washed in ice-cold PBS and resuspended in binding buffer containing annexin V and propidium iodide (Life Technologies). For the cell cycle assay, cells were washed with cold PBS, fixed with cold 100% ethanol, treated with RNase A, and stained with 10 μg/ml propidium iodide in PBS. A total of 100,000 events were collected on MacsQuant VYB (Miltenyi Biotec) and analyzed using FlowJo v10.1 (Tree Star).

Immunoblotting. Cells were treated with indicated concentration of inhibitors and lysed in radioimmunoprecipitation assay (RIPA) buffer supplemented with protease inhibitor cocktail (Roche), 30 mM β-glycerol phosphate, 50 mM sodium fluoride, and 1 mM sodium orthovanadate, incubated for 1 h on ice, and centrifuged at 14,000 × *g* for 5 min at 4°C. The protein concentration was determined by bicinchoninic acid (BCA) assay, and equal amounts of protein were loaded onto 10% SDS-polyacrylamide gel, separated by electrophoresis, and transferred to a polyvinylidene difluoride (PVDF) membrane (Sigma-Aldrich). The following primary antibodies were used at a 1:1,000 dilution: phospho-S6 ribosomal protein Ser240–244 (no. 2215), S6 ribosomal protein 5G10 (no. 2217), phospho-4E-BP1 Ser65 (no. 9451), 4E-BP1 (no. 9452), phospho-AKT Ser473 D93 XP (no. 4060), AKT pan-11E7 (no. 4685), phospho-NDGR1 Thr346 (no. 3217), NDRG1 D6C2 (no. 9408), cleaved caspase-3 Asp175 (no. 9664), and cleaved PARP

Asp214 D64E10 XP (no. 5625) from Cell Signaling and β-actin (A5441) from Sigma. Signal was detected with horseradish peroxidase (HRP)-conjugated secondary antibodies (Vector Labs) and developed using ECL enhanced chemiluminescence substrate (Pierce). Phosphorylated proteins were detected first, and then membranes were stripped with One Minute Advance Western blot stripping buffer (GM Biosciences) and probed for total protein.

ELISA. For enzyme-linked immunosorbent assay (ELISA), IL-6 and IL-10 were quantified using the Ready-Set-Go kit (eBioscience) per the manufacturer's instructions. Plates were washed with plate washer ELx405 (Biotek). Absorbance was measured at 450 nm using spectrophotometer Infinite M200 PRO (Tecan).

Kinome scan. DiscoveRx 442 kinome-wide selectivity profiling was conducted by DiscoveRx Bioscience with KinomeScan technology.

Xenograft studies. Six-week-old female NSG mice (Jackson Laboratory) were injected intraperitoneally (i.p.) with 1×10^5 cells. After 3 days, mice were randomized to a vehicle or treatment group, based on initial luminescent results before drug injections. MLN0128 and rapamycin were administered by i.p. or subcutaneous (s.c.) injections as indicated. The entire study group was euthanized when the vehicle group body score dropped below 2 or >20% loss of body weight. Effusion volumes were collected from the peritoneal cavity and measured. In mice that did not have any effusion to be collected, the cavity was washed with PBS to obtained PEL cells still present on the cavity. Effusions were diluted 1:3 with cold PBS with 2% FBS and centrifuged at $300 \times g$ for 5 min, and supernatant and cell pellets were flash frozen and stored at −80. For every experiment, $n = 5$ for each treatment group, based on power calculations to record statistically significant ($P \leq 0.05$) alterations for individual measures. All mouse studies were performed by the UNC Lineberger Animal Studies Core Facility; the investigator was not present during group randomization or outcome assessment of bioluminescent measurements and fluid collection.

Bioluminescent imaging. Bioluminescent imaging was performed using the Xenogen IVIS-Lumina system (Caliper Life Sciences). Mice were anesthetized using 2% isoflurane and 100% oxygen at a flow rate of 2.5 liters/min. Then 10 μl/g of a 15-mg/ml sterile D-luciferin firefly substrate (Biosynth International, Inc.) dissolved in PBS was administered by i.p. injection, and 15 min after substrate injection, the mice were imaged for up to 2 min. Each image was saved for subsequent analysis. The images were analyzed with Living Image 4.2. The scales to the right of the images in Fig. 4D represent the photon emission from the tissue surfaces and are expressed as photons per second per centimeter squared per steradian (p/s/cm^2/sr).

PET-CT imaging. MicroPET and micro-CT images were acquired with an eXplore Vista small animal PET-CT scanner (GE Healthcare) with a center resolution of 1.2 mm and a 46-mm axial field of view. Food was removed from mouse cages at least 4 h before radiotracer injection. Mice were anesthetized in an induction chamber with a 3% isoflurane–oxygen mixture (vol/vol) and then injected intravenously via tail vein catheter with approximately 300 μCi of ^{18}F-labeled fluorodeoxyglucose ([^{18}F]FDG). The syringe and catheter were then removed, and residue activity was measured and subtracted from the total injected activity. After the injection, mice were allowed to recover from anesthesia and placed back in the cage to resume activity. Approximately 45 min after injection of the radiotracer, mice were placed back in the induction chamber with 3% isoflurane, which was reduced to 1.5% for maintenance of anesthesia before the animal was placed prone on the PET cradle, with legs secured to the side. A respiratory monitor (SA Instruments, Inc., Stony Brook, NY) was placed above the animal. Temperature was monitored with an infrared thermometer and maintained with a heat lamp. A CT scan of the animal's abdominal region was then taken for attenuation correction and anatomical reference, with a tube current of 140 μA and voltage of 40 kVp. Sixty minutes after the injection of the radiotracer, a 20-min static PET scan of the abdominal region was acquired. PET emission data were corrected for decay/dead time and reconstructed with the Vista software, using a 2D ordered subset expectation maximization (2D-OSEM) algorithm that corrects for random coincidences, scatter, and attenuation and calibrates the image to standardized uptake value (SUV).

Drug resistance. Cell lines resistant to rapamycin (RR1, RR2, and RR3) were generated by exposing the parental PEL cell line, BCBL-1TrexRTA-Luc, to an increasing dose of rapamycin (up to 1,000 nM/100× IC_{50}) for 3 months. Clones were obtained by extracting and expanding a single colony from a colony formation assay. Clones were maintained at 100 nM rapamycin.

Exome sequencing and mutation calling analysis. Total nucleic acid was extracted from 1×10^6 cells using a MagNA Pure compact nucleic acid isolation kit I large-volume kit (Roche) and quantitated by Qubit 3.0 double-stranded DNA (dsDNA) high-sensitivity (HS) assay (Life Technologies). Barcoded exome sequencing libraries were prepared from 100 ng DNA with an Ion AmpliSeq Exome RDY library preparation kit (Life Technologies) using protocol MAN00009808 Rev: A.0. Libraries were quantitated by Qubit dsDNA HS assay, sized with an Agilent Bioanalyzer 2100 high-sensitivity DNA assay (Agilent Technologies), and pooled to 80 pM final concentration. Templating and loading onto the Ion 540 Chip (Life Technologies) were automated on the Ion Chef (Life Technologies). Samples were sequenced on the Ion S5 system (Life Technologies). Base calling, quality filtering, and demultiplexing were performed on the Ion S5 (Life Technologies) with default parameters. Raw reads were trimmed to >50 bp and mapped to the human genome (NCBI build hg38_2016) using CLC Genomics Workbench 9 (CLC bio). The CLC basic variant detection tool was used with the parameters minimum average quality score = 19, minimum frequency = 90%, and minimum coverage = 40. Only single-nucleotide polymorphism (SNP) calls with forward and reverse balance of $0.25 < x < 0.75$ were included in the analysis.

RNA-seq and analysis. Total RNA was purified and poly(A) enriched using Oligotex mRNA minikits (Qiagen). Library preparation was performed according to the Ion total RNA-Seq kit v2 whole-transcriptome RNA protocol (ThermoFisher Scientific, publication no. MAN0010654, revision B.0) with the

following modifications: purification of fragmented RNA and cDNA was with 1.8× Agencourt RNAClean XP beads (Beckman Coulter, Inc.) (*Ovation Universal RNA-Seq System User Guide*; NuGEN), and an additional Agencourt AMPure XP 1.0× bead (Beckman Coulter, Inc.) cleanup of the finished library was performed. Libraries were quality controlled and quantitated using the 2100 high-sensitivity DNA assay (Agilent Technologies) and Qubit dsDNA HS assay (ThermoFisher Scientific). A 50 pM concentration of library was templated on the Ion Torrent Chef for 200 bp and sequenced on the Ion Torrent S5 using a 540 chip. Subsequent steps included quality control using bbduk version 37.25 (k = 23 mink = 11 ktrim=r hdist = 1 minlength = 100 qtrim=rl trimq = 20 ftl = 10 ftr = 600 maq = 20 tpe tbo), mapping to reference genome (GRCh38, STAR aligner v2.5.3a, gencode v22 annotations), with read counting on genes (summarizeOverlaps, mode: intersection-strict, singleEnd). Differential gene expression was calculated using DESeq2 working with a simple interaction term for the model: design = ~ Drug + Clone.Number. PCA, distance heat maps, and other figures were generated in R using DESeq2 and ggplot2. Genes were considered differentially expressed by the Wald test, with an adjusted (Benjamini-Hochberg) P value of <0.05.

Statistics. Results are reported as mean ± standard deviation (SD). All cellular experiments were repeated in at least three complete biological replicates. The unpaired 2-tailed t test with Welch correction (do not assume equal SD) was used to statistically compare groups.

Code availability. For drug-response curves, the public DRC package version 3.0 from R was used. The package is available at https://cran.r-project.org/web/packages/drc/index.html.

Study approval. Studies were approved by the IACUC of the University of North Carolina, Chapel Hill, NC.

Data availability. Raw sequences have been deposited under NCBI BioProject accession no. PRJNA414221. The complete code for analysis and gene list have been deposited in bitbucket (https://ddittmer@bitbucket.org/dittmerlab/rapamycin_mln0128_resistance_rnaseq.git).

SUPPLEMENTAL MATERIAL

Supplemental material for this article may be found at https://doi.org/10.1128/mBio.02871-18.

FIG S1, DOCX file, 0.7 MB.
FIG S2, DOCX file, 0.2 MB.
FIG S3, DOCX file, 0.3 MB.
FIG S4, DOCX file, 1.2 MB.
FIG S5, DOCX file, 1 MB.
FIG S6, DOCX file, 0.2 MB.
FIG S7, DOCX file, 0.3 MB.
TABLE S1, XLSX file, 0.1 MB.
MOVIE S1, MOV file, 0.8 MB.
MOVIE S2, MOV file, 0.7 MB.

ACKNOWLEDGMENTS

This work was supported by Public Health Service grant CA163217 to D.P.D. and B.D. Animal Studies were performed within the UNC Lineberger Animal Studies Core Facility at the University of North Carolina at Chapel Hill. The UNC Lineberger Animal Studies Core and the Small Animal Imaging Core facility at the UNC Biomedical Imaging Research Center are supported in part by NCI cancer center grant CA016086. The Vironomics Core at the University of North Carolina at Chapel Hill provided the exome sequencing and RNA sequencing services.

We thank Hyowon An and Justin Landis for assistance with R coding.

C.C.-V. designed and performed experiments, analyzed data, and wrote the manuscript. A.B. analyzed data. R.B. generated the BCBL-1TrexRTA-Luc cell line and provided critical analysis. B.D. designed experiments and contributed to the final version of the manuscript. D.P.D. designed experiments, analyzed data, and contributed to the final version of the manuscript. All authors approved the final manuscript.

The authors have declared that no conflict of interest exists.

REFERENCES

1. Cesarman E, Chang Y, Moore PS, Said JW, Knowles DM. 1995. Kaposi's sarcoma-associated herpesvirus-like DNA sequences in AIDS-related body-cavity-based lymphomas. N Engl J Med 332:1186–1191. https://doi.org/10.1056/NEJM199505043321802.
2. Jones D, Ballestas ME, Kaye KM, Gulizia JM, Winters GL, Fletcher J, Scadden DT, Aster JC. 1998. Primary-effusion lymphoma and Kaposi's sarcoma in a cardiac-transplant recipient. N Engl J Med 339:444–449. https://doi.org/10.1056/NEJM199808133390705.
3. Boulanger E, Gerard L, Gabarre J, Molina JM, Rapp C, Abino JF, Cadranel J, Chevret S, Oksenhendler E. 2005. Prognostic factors and outcome of

human herpesvirus 8-associated primary effusion lymphoma in patients with AIDS. J Clin Oncol 23:4372–4380. https://doi.org/10.1200/JCO.2005.07.084.

4. Komanduri KV, Luce JA, McGrath MS, Herndier BG, Ng VL. 1996. The natural history and molecular heterogeneity of HIV-associated primary malignant lymphomatous effusions. J Acquir Immune Defic Syndr Hum Retrovirol 13:215–226.
5. Sin SH, Roy D, Wang L, Staudt MR, Fakhari FD, Patel DD, Henry D, Harrington WJ, Jr, Damania BA, Dittmer DP. 2007. Rapamycin is efficacious against primary effusion lymphoma (PEL) cell lines in vivo by inhibiting autocrine signaling. Blood 109:2165–2173. https://doi.org/10.1182/blood-2006-06-028092.
6. Bhatt AP, Bhende PM, Sin SH, Roy D, Dittmer DP, Damania B. 2010. Dual inhibition of PI3K and mTOR inhibits autocrine and paracrine proliferative loops in PI3K/Akt/mTOR-addicted lymphomas. Blood 115:4455–4463. https://doi.org/10.1182/blood-2009-10-251082.
7. Saxton RA, Sabatini DM. 2017. mTOR signaling in growth, metabolism, and disease. Cell 168:960–976. https://doi.org/10.1016/j.cell.2017.02.004.
8. Roy D, Dittmer DP. 2011. Phosphatase and tensin homolog on chromosome 10 is phosphorylated in primary effusion lymphoma and Kaposi's sarcoma. Am J Pathol 179:2108–2119. https://doi.org/10.1016/j.ajpath.2011.06.017.
9. Tomlinson CC, Damania B. 2004. The K1 protein of Kaposi's sarcoma-associated herpesvirus activates the Akt signaling pathway. J Virol 78:1918–1927. https://doi.org/10.1128/JVI.78.4.1918-1927.2004.
10. Kuang E, Tang Q, Maul GG, Zhu F. 2008. Activation of p90 ribosomal S6 kinase by ORF45 of Kaposi's sarcoma-associated herpesvirus and its role in viral lytic replication. J Virol 82:1838–1850. https://doi.org/10.1128/JVI.02119-07.
11. Morris VA, Punjabi AS, Lagunoff M. 2008. Activation of Akt through gp130 receptor signaling is required for Kaposi's sarcoma-associated herpesvirus-induced lymphatic reprogramming of endothelial cells. J Virol 82:8771–8779. https://doi.org/10.1128/JVI.00766-08.
12. Sodhi A, Chaisuparat R, Hu J, Ramsdell AK, Manning BD, Sausville EA, Sawai ET, Molinolo A, Gutkind JS, Montaner S. 2006. The TSC2/mTOR pathway drives endothelial cell transformation induced by the Kaposi's sarcoma-associated herpesvirus G protein-coupled receptor. Cancer Cell 10:133–143. https://doi.org/10.1016/j.ccr.2006.05.026.
13. Sodhi A, Montaner S, Patel V, Gomez-Roman JJ, Li Y, Sausville EA, Sawai ET, Gutkind JS. 2004. Akt plays a central role in sarcomagenesis induced by Kaposi's sarcoma herpesvirus-encoded G protein-coupled receptor. Proc Natl Acad Sci U S A 101:4821–4826. https://doi.org/10.1073/pnas.0400835101.
14. Hara K, Maruki Y, Long X, Yoshino K, Oshiro N, Hidayat S, Tokunaga C, Avruch J, Yonezawa K. 2002. Raptor, a binding partner of target of rapamycin (TOR), mediates TOR action. Cell 110:177–189.
15. Kim DH, Sarbassov DD, Ali SM, King JE, Latek RR, Erdjument-Bromage H, Tempst P, Sabatini DM. 2002. mTOR interacts with raptor to form a nutrient-sensitive complex that signals to the cell growth machinery. Cell 110:163–175. https://doi.org/10.1016/S0092-8674(02)00808-5.
16. Sarbassov DD, Ali SM, Kim DH, Guertin DA, Latek RR, Erdjument-Bromage H, Tempst P, Sabatini DM. 2004. Rictor, a novel binding partner of mTOR, defines a rapamycin-insensitive and raptor-independent pathway that regulates the cytoskeleton. Curr Biol 14:1296–1302. https://doi.org/10.1016/j.cub.2004.06.054.
17. Jacinto E, Loewith R, Schmidt A, Lin S, Ruegg MA, Hall A, Hall MN. 2004. Mammalian TOR complex 2 controls the actin cytoskeleton and is rapamycin insensitive. Nat Cell Biol 6:1122–1128. https://doi.org/10.1038/ncb1183.
18. Magnuson B, Ekim B, Fingar DC. 2012. Regulation and function of ribosomal protein S6 kinase (S6K) within mTOR signalling networks. Biochem J 441:1–21. https://doi.org/10.1042/BJ20110892.
19. Sarbassov DD, Guertin DA, Ali SM, Sabatini DM. 2005. Phosphorylation and regulation of Akt/PKB by the rictor-mTOR complex. Science 307:1098–1101. https://doi.org/10.1126/science.1106148.
20. Guertin DA, Stevens DM, Thoreen CC, Burds AA, Kalaany NY, Moffat J, Brown M, Fitzgerald KJ, Sabatini DM. 2006. Ablation in mice of the mTORC components raptor, rictor, or mLST8 reveals that mTORC2 is required for signaling to Akt-FOXO and PKCalpha, but not S6K1. Dev Cell 11:859–871. https://doi.org/10.1016/j.devcel.2006.10.007.
21. García-Martínez JM, Alessi DR. 2008. mTOR complex 2 (mTORC2) controls hydrophobic motif phosphorylation and activation of serum- and glucocorticoid-induced protein kinase 1 (SGK1). Biochem J 416:375–385. https://doi.org/10.1042/BJ20081668.
22. Zhang L, Cui R, Cheng X, Du J. 2005. Antiapoptotic effect of serum and glucocorticoid-inducible protein kinase is mediated by novel mechanism activating IκB kinase. Cancer Res 65:457–464.
23. Murray JT, Campbell DG, Morrice N, Auld GC, Shpiro N, Marquez R, Peggie M, Bain J, Bloomberg GB, Grahammer F, Lang F, Wulff P, Kuhl D, Cohen P. 2004. Exploitation of KESTREL to identify NDRG family members as physiological substrates for SGK1 and GSK3. Biochem J 384:477–488. https://doi.org/10.1042/BJ20041057.
24. Krown SE, Roy D, Lee JY, Dezube BJ, Reid EG, Venkataramanan R, Han K, Cesarman E, Dittmer DP. 2012. Rapamycin with antiretroviral therapy in AIDS-associated Kaposi sarcoma: an AIDS Malignancy Consortium study. J Acquir Immune Defic Syndr 59:447–454. https://doi.org/10.1097/QAI.0b013e31823e7884.
25. Roy D, Sin SH, Lucas A, Venkataramanan R, Wang L, Eason A, Chavakula V, Hilton IB, Tamburro KM, Damania B, Dittmer DP. 2013. mTOR inhibitors block Kaposi sarcoma growth by inhibiting essential autocrine growth factors and tumor angiogenesis. Cancer Res 73:2235–2246. https://doi.org/10.1158/0008-5472.CAN-12-1851.
26. Stallone G, Schena A, Infante B, Di Paolo S, Loverre A, Maggio G, Ranieri E, Gesualdo L, Schena FP, Grandaliano G. 2005. Sirolimus for Kaposi's sarcoma in renal-transplant recipients. N Engl J Med 352:1317–1323. https://doi.org/10.1056/NEJMoa042831.
27. Gasperini P, Tosato G. 2009. Targeting the mammalian target of rapamycin to inhibit VEGF and cytokines for the treatment of primary effusion lymphoma. Leukemia 23:1867–1874. https://doi.org/10.1038/leu.2009.117.
28. Thoreen CC, Sabatini DM. 2009. Rapamycin inhibits mTORC1, but not completely. Autophagy 5:725–726. https://doi.org/10.4161/auto.5.5.8504.
29. Choo AY, Yoon SO, Kim SG, Roux PP, Blenis J. 2008. Rapamycin differentially inhibits S6Ks and 4E-BP1 to mediate cell-type-specific repression of mRNA translation. Proc Natl Acad Sci U S A 105:17414–17419. https://doi.org/10.1073/pnas.0809136105.
30. Feldman ME, Apsel B, Uotila A, Loewith R, Knight ZA, Ruggero D, Shokat KM. 2009. Active-site inhibitors of mTOR target rapamycin-resistant outputs of mTORC1 and mTORC2. PLoS Biol 7:e38. https://doi.org/10.1371/journal.pbio.1000038.
31. O'Reilly KE, Rojo F, She QB, Solit D, Mills GB, Smith D, Lane H, Hofmann F, Hicklin DJ, Ludwig DL, Baselga J, Rosen N. 2006. mTOR inhibition induces upstream receptor tyrosine kinase signaling and activates Akt. Cancer Res 66:1500–1508. https://doi.org/10.1158/0008-5472.CAN-05-2925.
32. Ghobrial IM, Siegel DS, Vij R, Berdeja JG, Richardson PG, Neuwirth R, Patel CG, Zohren F, Wolf JL. 2016. TAK-228 (formerly MLN0128), an investigational oral dual TORC1/2 inhibitor: a phase I dose escalation study in patients with relapsed or refractory multiple myeloma, non-Hodgkin lymphoma, or Waldenstrom's macroglobulinemia. Am J Hematol 91:400–405. https://doi.org/10.1002/ajh.24300.
33. Kunati SR, Xu Y. 2017. Determination of MLN0128, an investigational antineoplastic agent, in human plasma by LC-MS/MS. Biomed Chromatogr 31:e3818. https://doi.org/10.1002/bmc.3818.
34. Burris HA, III, Kurkjian CD, Hart L, Pant S, Murphy PB, Jones SF, Neuwirth R, Patel CG, Zohren F, Infante JR. 2017. TAK-228 (formerly MLN0128), an investigational dual TORC1/2 inhibitor plus paclitaxel, with/without trastuzumab, in patients with advanced solid malignancies. Cancer Chemother Pharmacol 80:261–273. https://doi.org/10.1007/s00280-017-3343-4.
35. Carbone A, Cesarman E, Gloghini A, Drexler HG. 2010. Understanding pathogenetic aspects and clinical presentation of primary effusion lymphoma through its derived cell lines. AIDS 24:479–490. https://doi.org/10.1097/QAD.0b013e3283365395.
36. Drexler HG, Meyer C, Gaidano G, Carbone A. 1999. Constitutive cytokine production by primary effusion (body cavity-based) lymphoma-derived cell lines. Leukemia 13:634–640.
37. Liu Q, Kirubakaran S, Hur W, Niepel M, Westover K, Thoreen CC, Wang J, Ni J, Patricelli MP, Vogel K, Riddle S, Waller DL, Traynor R, Sanda T, Zhao Z, Kang SA, Zhao J, Look AT, Sorger PK, Sabatini DM, Gray NS. 2012. Kinome-wide selectivity profiling of ATP-competitive mammalian target of rapamycin (mTOR) inhibitors and characterization of their binding kinetics. J Biol Chem 287:9742–9752. https://doi.org/10.1074/jbc.M111.304485.
38. Yang H, Rudge DG, Koos JD, Vaidialingam B, Yang HJ, Pavletich NP. 2013.

mTOR kinase structure, mechanism and regulation. Nature 497:217–223. https://doi.org/10.1038/nature12122.
39. Carlo MI, Molina AM, Lakhman Y, Patil S, Woo K, DeLuca J, Lee CH, Hsieh JJ, Feldman DR, Motzer RJ, Voss MH. 2016. A phase Ib study of BEZ235, a dual inhibitor of phosphatidylinositol 3-kinase (PI3K) and mammalian target of rapamycin (mTOR), in patients with advanced renal cell carcinoma. Oncologist 21:787–788. https://doi.org/10.1634/theoncologist.2016-0145.
40. Seront E, Rottey S, Filleul B, Glorieux P, Goeminne JC, Verschaeve V, Vandenbulcke JM, Sautois B, Boegner P, Gillain A, van Maanen A, Machiels JP. 2016. Phase II study of dual phosphoinositol-3-kinase (PI3K) and mammalian target of rapamycin (mTOR) inhibitor BEZ235 in patients with locally advanced or metastatic transitional cell carcinoma. BJU Int 118:408–415. https://doi.org/10.1111/bju.13415.
41. Motzer RJ, Escudier B, Oudard S, Hutson TE, Porta C, Bracarda S, Grunwald V, Thompson JA, Figlin RA, Hollaender N, Urbanowitz G, Berg WJ, Kay A, Lebwohl D, Ravaud A, RECORD-1 Study Group. 2008. Efficacy of everolimus in advanced renal cell carcinoma: a double-blind, randomised, placebo-controlled phase III trial. Lancet 372:449–456. https://doi.org/10.1016/S0140-6736(08)61039-9.
42. Petre CE, Sin SH, Dittmer DP. 2007. Functional p53 signaling in Kaposi's sarcoma-associated herpesvirus lymphomas: implications for therapy. J Virol 81:1912–1922. https://doi.org/10.1128/JVI.01757-06.
43. Nichols LA, Adang LA, Kedes DH. 2011. Rapamycin blocks production of KSHV/HHV8: insights into the anti-tumor activity of an immunosuppressant drug. PLoS One 6:e14535. https://doi.org/10.1371/journal.pone.0014535.
44. Bhatt AP, Wong JP, Weinberg MS, Host KM, Giffin LC, Buijnink J, van Dijk E, Izumiya Y, Kung HJ, Temple BR, Damania B. 2016. A viral kinase mimics S6 kinase to enhance cell proliferation. Proc Natl Acad Sci U S A 113:7876–7881. https://doi.org/10.1073/pnas.1600587113.
45. Brown VI, Fang J, Alcorn K, Barr R, Kim JM, Wasserman R, Grupp SA. 2003. Rapamycin is active against B-precursor leukemia in vitro and in vivo, an effect that is modulated by IL-7-mediated signaling. Proc Natl Acad Sci U S A 100:15113–15118. https://doi.org/10.1073/pnas.2436348100.
46. Nakamura H, Lu M, Gwack Y, Souvlis J, Zeichner SL, Jung JU. 2003. Global changes in Kaposi's sarcoma-associated virus gene expression patterns following expression of a tetracycline-inducible Rta transactivator. J Virol 77:4205–4220.